Geophysical Research Letters

RESEARCH LETTER
10.1029/2019GL082394

Evidence for High Rates of Gas Transport in the Deep Subsurface

P. H. Stauffer[1], T. Rahn[2], J. P. Ortiz[1], L. J. Salazar[3], H. Boukhalfa[2], H. R. Behar[4], and E. E. Snyder[5]

[1]Los Alamos National Laboratory, EES-16 Computational Earth Sciences, Los Alamos, New Mexico, USA, [2]Los Alamos National Laboratory, EES-14 Earth Systems Observations, Los Alamos, New Mexico, USA, [3]N3B Los Alamos, Los Alamos, New Mexico, USA, [4]Water Resources Science Graduate Program, University of Minnesota, Duluth, Minnesota, USA, [5]Department of Earth and Environmental Science, New Mexico Institute of Mining and Technology, Socorro, New Mexico, USA

Key Points:
- Barometric pumping can induce significant gas flow and transport in deep fractured media
- Tracer testing helps characterize subsurface permeability, porosity, and diffusivity
- Simulations elucidate barometrically induced spreading of gas constituents in fractured rock and can aid in predictions of gas releases

Supporting Information:
- Supporting Information S1

Correspondence to:
P. H. Stauffer,
stauffer@lanl.gov

Citation:
Stauffer, P. H., Rahn, T., Ortiz, J. P., Salazar, L. J., Boukhalfa, H., Behar, H. R., & Snyder, E. E. (2019). Evidence for high rates of gas transport in the deep subsurface. *Geophysical Research Letters*, *46*. https://doi.org/10.1029/2019GL082394

Received 7 FEB 2019
Accepted 14 MAR 2019
Accepted article online 18 MAR 2019

Abstract Barometric pumping caused by atmospheric pressure fluctuations contributes to the motion of gases in the vadose zone. While the resulting gas transport is often negligible in unfractured porous rocks, rates of transport in fractured media can be significant. Deep atmospheric pumping has implications for nuclear gas detection, water balance, and contaminant transport. We present results from a tracer test conducted to characterize deep subsurface fractured basalt and investigate the effects of barometric pumping on gaseous contaminant mobility. The tracer test provides data to constrain permeability, porosity, and diffusivity in a numerical representation of the experiment. A numerical model is used to simulate gas flow and dispersive transport under fluctuating pressure conditions. Tracer test and simulation results suggest that barometric pumping induces 10 to 100 times more mixing in the basalt than predicted by gas diffusion alone. Within the basalt fractures, estimates of gas velocity reach maximums of nearly 1,000 m/day.

Plain Language Summary Weather systems have associated changes in atmospheric pressure. Storm systems bring low pressure and blue skies bring high pressure. These changes in pressure are also imposed on the soils and rocks beneath our feet. If the soils and rocks have sufficient open pore space or well-connected fractures, atmospheric pressure changes can drive air into or pull air out of these geologic materials. This phenomenon is known as barometric pumping. Barometric pumping can accelerate the migration of natural or man-made gases. In this study, we have investigated the effects of barometric pumping on a highly fractured geologic formation that underlies the Los Alamos National Laboratory. To do so, we injected a nonreactive tracer gas called sulfur hexafluoride and monitored its concentration over time for several days. These measurements are used to constrain simulations that take into account the fractured nature of the geologic formation. We have determined that barometric pumping has a significant influence on this particular geologic formation and discovered that gases may travel at rates of up to a kilometer per day for brief periods, much higher than the tens of centimeters per day possible if the gases were dispersed by simple molecular diffusion.

1. Introduction

Atmospheric pressure fluctuations contribute to the motion of gases in the vadose zone. Periods of high atmospheric pressure push gases downward into the subsurface, while periods of low pressure draw gases upward toward the surface (Nilson et al., 1991). Barometric pumping has been investigated thoroughly in the literature (Kuang et al., 2013; Scotter et al., 1967; Scotter & Raats, 1968; You et al., 2011)), and has been used to characterize the subsurface (Neeper, 2002; Rossabi, 2006). Broadly, barometric pumping has been shown to impact the mobility of volatile organic compounds (VOCs; Auer et al., 1996; Neeper & Stauffer, 2012a, 2012b; You & Zhan, 2013) and radionuclide gases (Bourret et al., 2018; Carrigan et al., 1996; Harp et al., 2018; Jordan et al., 2015). Deep drying and subsequent reductions in infiltration fluxes are hypothesized to result from pumping of dry air through fractured rock (Weeks, 2001).

The effects of barometric pumping on transport processes may be orders of magnitude greater in fractured media than in homogeneous, unfractured porous media (Nilson et al., 1991; Carrigan et al., 1996). In a case described by Auer et al. (1996), gas velocity in an unfractured, homogeneous system with barometric

pumping was calculated to be on the order of 10^{-6} to 10^{-5} m/s, or 0.1 to 1 m/day. Gas velocities in the fractured vadose zone of Yucca Mountain, where barometric pumping effects are well documented, have been calculated as 0.03 m/s, or 2,600 m/day (Martinez & Nilson, 1999). Also at Yucca Mountain, airflow speeds of 3 m/s have been measured in open boreholes; however, borehole flow integrates gas flow over the open interval of the borehole and is not directly scalable to fracture velocities within the mountain. These gas velocity estimates provide insight into previously measured ranges and further illustrate how barometric pumping may impact atmospheric gas flow in the deep vadose zone.

In this paper, we present a gas tracer test conducted to characterize subsurface basalt and investigate the effects of barometric pumping on gas transport in the deep subsurface. The tracer test was conducted at Material Disposal Area L (MDA L), the site of a subsurface VOC vapor plume (Figure S1) at Los Alamos National Laboratory (LANL) in New Mexico, USA. While VOC movement within the tuff units that contain the plume can be understood using a diffusive transport model, there remains considerable uncertainty regarding the transport of vapors through the deep, underlying fractured and rubblized basalt (Behar et al., 2018; Stauffer et al., 2005). To address this uncertainty, we employ data from the tracer test to develop a numerical model that simulates gas flow and tracer transport in the deep basalt under barometric pumping conditions. The resulting simulations that honor both time-dependent pressure and tracer dilution data are used to validate our conceptual model and transport hypotheses and have broad significance to gas transport in deep unsaturated systems. The scale of the numerical analysis is limited to include a region sufficient to demonstrate processes that may impact gas transport in deep, fractured systems.

1.1. Site Background

MDA L operated from the 1960s to 1985 as a liquid chemical waste disposal site (Stauffer et al., 2005). Waste drums emplaced in shafts subsequently leaked, forming a subsurface VOC vapor plume that extends beyond the boundaries of the 2.5 acre MDA L site and to a depth of approximately 90 m (Behar et al., 2018). Monitoring boreholes show 1,1,1-tricholorethane as the primary plume constituent. Borehole 54-24399 was installed in 2005 near the center of MDA L (Figure S1) and has been used to sample VOC concentrations in the deep Cerros del Rio basalt. A dedicated, permanent packer system and sampling line are used to collect samples from two ports located at 173 and 179 m deep in borehole 54-24399.

1.2. Site Hydrology

The MDA L site is located on Mesita del Buey, a narrow finger mesa of the Pajarito Plateau in New Mexico, USA. The mesa is bounded by canyons: Cañada del Buey to the north and Pajarito Canyon to the south (Stauffer et al., 2005). The plateau was formed between 1.6 and 2.8 Ma (million years ago) by eruptions of the Cerros del Rio (2.3 and 2.8 Ma) and Jemez (1.6 Ma) volcanic fields (Broxton & Vaniman, 2005). The Cerros del Rio eruptions formed the Cerros del Rio basalt (Tb4), which is the deepest geologic unit of the unsaturated zone and varies in composition from low porosity, to vesicular, to highly fractured rock (Broxton & Vaniman, 2005; Figure S2). Eruptions of the Jemez volcanic field formed the overlying Bandelier Tuff (Broxton & Vaniman, 2005). The water table is at a depth of approximately 285 m below ground surface (bgs).

Theoretical and numerical reasoning combined with field observations have led to the conclusion that the Cerros del Rio basalt is highly permeable and connected with the atmosphere. When borehole 54-01016 was drilled into the basalt, drilling air emerged at nearby borehole 54-01015. Further calculations based on pressure differences between boreholes 54-01015 and 54-01016 suggest that the basalt permeability exceeds 10^{-9} m^2 at depth > 100 m bgs (Neeper, 2002). Field measurements have also shown that pressure variations in the basalt are damped less than pressure variations in the overlying tuff (Neeper, 2002, Figure 8). This indicates that the basalt is extremely conductive to airflow from outcrops such as those to the east of MDA L (Figure S3). Barometric pumping in the Cerros del Rio basalt generates 1–2-kPa variations in subsurface pressure, inducing oscillatory flow and creating an effective diffusivity that could be orders of magnitude larger than pure gas diffusion (Auer et al., 1996; Neeper, 2002).

2. Tracer Test Methods

Gas tracer tests were conducted using SF_6, a nonreactive and poorly soluble tracer that allows observation of gas flow without interaction with water. To determine background SF_6 concentration prior to the tracer test,

LANL analyzed data from a field-deployed Photoacoustic Gas Monitor (LumaSense model no. INNOVA 1412i, hereafter, INNOVA) at borehole 54-24399. LANL also collected gas samples from boreholes 54-01015 and 54-01016. Analysis of the gas samples collected prior to injection showed that background SF_6 in the deep basalt is below the INNOVA detection limit of 10 ppb.

Starting on 5 April 2017, a 1-L bag (5-g aliquot) of gas tracer SF_6 was injected into borehole 54-24399 at a depth of 173 m through the injection/return flow tubing of the packer system (Figures S4 and S5). The tracer was subsequently monitored as it spread into the subsurface. Flow of about 2 L per minute to the packer outlet was continued for 10 min to ensure that the entire volume of tracer was flushed through the downhole tubing (approximate volume 2 L). After injection and flushing of the tubing to 173 m bgs, the pump was reversed and sampling was initiated with the INNOVA from 173 m bgs. INNOVA data were recorded approximately every 57 s.

2.1. Analytical Instruments

The INNOVA unit was equipped with an infrared light source and a sequence of band-pass filters for SF_6, CO_2, tetrachloroethylene, trichloroethane, and H_2O. Instrument flow rate was approximately 2 L per minute and response time was ~1 min for the full suite of analytes. For the gas phase of interest, SF_6, the instrument detection limit reported by the manufacturer is on the order of ~10 nmol/mol. The instrument was factory calibrated immediately prior to field deployment and tested with in-house standards at 0.1, 1.0, and 10 μmol/mol SF_6 (Figure S6). Instrument response with in-house standards was linear over the range tested with accuracy of better than 1% of the measured value.

2.2. Pressure and Temperature Measurements

Pressure data were recorded prior to and during the tracer injection test. Pressure was recorded at the surface and in the tracer sampling zone of borehole 54-24399 at the base of the packer with absolute pressure gauges (omega absolute pressure gauges part nos. PX409-015AI-EH at the surface and PX429-015AI-EH at the packer, 0.08% accuracy). Transducers were scanned every second and averaged over 6-min intervals. Transducer excitation and logging of pressure data were performed with a Campbell Scientific data logger (model no. CR5000). Temperature logs were downloaded from LANL's observational weather tower and also collected from the internal INNOVA temperature sensor.

3. Tracer Test Results

3.1. Pressure Results

Between 3 and 17 April 2017, surface pressure varied between 784- and 800-hPa absolute pressure (Figure S7). Daily cycling of pressure with midday highs and nighttime lows having an amplitude of 3 to 5 hPa was overlain by low- and high-pressure periods driven by synoptic-scale weather patterns. These longer-period oscillations lasted one to several days and imposed an amplitude of 10 to 15 hPa on the surface pressure signal. Data recorded at depth revealed similar patterns but with less high-frequency variation and a lower amplitude in the diel variation of 2 to 3 hPa. The amplitude of synoptic forcing was more similar to the amplitude observed at the surface, that is, 10 to 15 hPa. These details can be observed in Figure 1 where surface pressure has been altitude adjusted by 173 m for comparison to downhole pressure. Another pattern to note is the phase shift (time lag)—typically on the order of 2 to 3 hr—of the downhole pressure relative to the atmospheric forcing (Figure 1). The result is an altitude adjusted difference of atmospheric to downhole pressure that varies from positive ~6 to −4 hPa (Figure S8).

3.2. Data Gaps

During the course of the tracer test, there were several periods where the sampling system integrity was compromised. These periods were the result of a variety of causes (e.g., periods where power to the pumps was lost, times when the system plumbing had to be opened to exchange desiccant). These periods hold the potential to yield erroneous results from the INNOVA. Observation of CO_2, which is produced at depth by microbial respiration, allows us to filter data that might be compromised. Any time that typical subsurface CO_2 concentration values of 1,400 μmol/mol approach atmospheric background values of 400 μmol/mol, we consider that SF_6 likewise has been diluted and is therefore not a reliable measurement of the true downhole concentration (Text S1 and Figure S9).

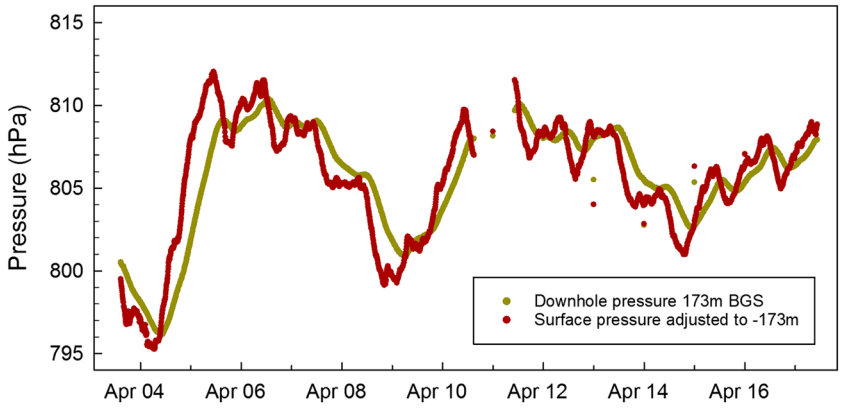

Figure 1. Measured surface pressure (red) adjusted to the same mean value as measured downhole pressure (gold) at 173 m bgs.

3.3. Sulfur Hexafluoride Results

SF_6 concentrations from the borehole are shown as a 10-min running average (Figure 2). An initial drop from 150 to 0.01 μmol/mol is followed by a recovery to a mole fraction of several tenths μmol/mol before concentrations appear to level off at between 0.02 and 0.05 μmol/mol. The behavior of the measured tracer response is not similar to pure diffusion, where concentrations would drop monotonically from the initial injection.

4. Numerical Modeling

Data collected during the tracer experiment are next used to create a numerical representation of the experiment. The model is built within the FEHM (Finite Element Heat and Mass) porous-flow simulator, developed at LANL, and used successfully to simulate barometrically pumped contaminant transport in fractured rock (Harp et al., 2018; Jordan et al., 2014, 2015; Neeper & Stauffer, 2012a, 2012b). FEHM simulates gas advection coupled to tracer transport using a standard form of the advection-dispersion equation (FEHM, 2019; Johnson, Otto, et al., 2019, Johnson, Zyvoloski, et al., 2019). The tracer test data can help to constrain aspects of the physical system such as permeability, porosity, and dispersivity. Previous publications describing simulations of the MDA L plume can be found in Stauffer et al. (2005) and Behar et al. (2018).

4.1. Model Domain

The 3-D geometry of the simulated system consists of an interval spanning the distance from the bottom of the deeper sampling port (179-m depth) to 2 m above the upper sampling port (171-m depth). The domain is 8 m in the vertical direction and 20 m wide, centered on the borehole and sampling ports (Figure S10). The domain is divided into two rock types, massive basalt with very low porosity and rubblized basalt with high porosity. The mesh includes a high-resolution borehole with a central radius of 0.07 m. The borehole runs the entire 8-m vertical length of the domain, with the upper 3.5 m of the borehole set to impermeable and non-diffusive, representing a cased/cemented interval. Porosity in the open section of the borehole is set to 0.999, while permeability in this section is fixed at 10^{-4} m^2 based on downhole pressure loss matching.

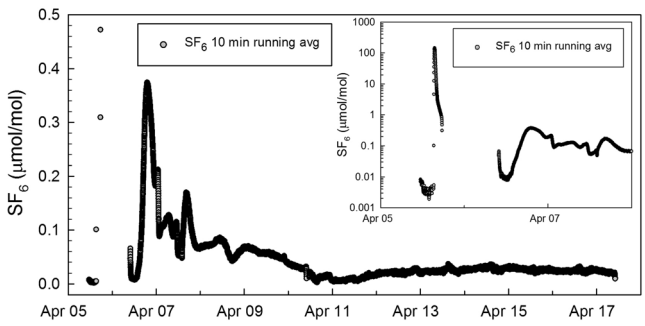

Figure 2. SF_6 data collected with the INNOVA from 5 to 17 April 2017. Inset is a log plot of concentration for the initial two days after injection.

The third dimension of the mesh extends from 0 to 2,500 m, with borehole 54-24399 located at 1,100 m (Figure S11). The 2,500-m mesh allows the boundaries to be adjusted such that the measured atmospheric forcing can be moved to the point at which the measured pressure response beneath the packer is recreated in the simulations. Mesh spacing is 1 m in all directions within 100 m on either side of the borehole. Past this central higher-resolution section, mesh spacing increases geometrically

to a maximum y spacing of approximately 10 m. Spacing in the x-z plane remains 1 m throughout the mesh. In Figure S11, $y = 0$ is on the right edge, while the wellbore shown in blue is located at $y = 1{,}100$ m. The atmospheric boundary condition can be moved closer or farther from the wellbore to a maximum distance of 1,400 m at the far boundary where $y = 2{,}500$ m.

4.2. Material Properties

To explore the potential for barometrically induced spreading in the basalt, we have based our initial conceptual model on the work of Neeper (2002). In this work, a fit to pressure data from boreholes 54-01015 and 54-01016 was used to estimate properties of the subsurface, including permeability, porosity, and the distances to atmospheric outcrops. Neeper found that to match the pressure response between these two wells, a 1-D analytical model required an outcrop located on order of 1.5 km from the wells, and a relationship between porosity (φ) and permeability (k) such that

$$k/\varphi = 2.2\times10^{-8}$$

The porosity of the rubblized basalt was assumed to be 35% (Vesselinov et al., 2002), leading to an estimated 7.7×10^{-9} m^2 permeability, or over 7,000 darcies. For the massive basalt, where flow is primarily through fractures, we use the cubic law (Mourzenko et al., 2014; Witherspoon et al., 1980) that relates aperture (a) to fracture permeability (k_f) as

$$k_f = a^2/12$$

From this function, the bulk permeability of a porous medium can be estimated assuming a parallel fracture model with one fracture of aperture (a) per meter as

$$k = a^3/12$$

For the simulations presented, an aperture of 4 mm was assumed, leading to a bulk permeability of the massive basalt of 5.3×10^{-9} m^2 and a corresponding porosity of 0.004.

4.3. Boundary Conditions

In Text S2, we present our efforts to address uncertainty in the dimensions of the domain and determine the scale and configuration of the domain used for numerical simulations of transport. Analytical and numerical modeling done as part of this study places the atmospheric boundary close to 1 km from borehole 54-24399, and this distance is used in the simulations presented.

Using a global tolerance of 10^{-10}, and a maximum mass transfer time step of 0.052 days, the simulation is initialized with a one-month pressure history from TA-54 adjusted to the correct elevation such that the mean of the weather station data are set equal to the mean of the data collected from the borehole transducer located beneath the packer (Figure S12). As shown, the atmospheric pressure driver used in FEHM exactly captures the measured data from the TA54 weather station.

4.4. Simulated Pressure Response at Depth

The next test of the simulation is to determine the distance at which the simulated pressure response at 173-m depth produces similar behavior to the measured pressure response. With the simplified domain used for the current study, we do not expect to completely capture the intricate behavior of a large 3-D system driven by atmospheric connections originating in many directions. However, by generating a numerical representation of the pressure variation at depth, driven by atmospheric pressure from a distant boundary, we can have confidence that the bulk airflow component of the simulation is recreating measured conditions. The atmospheric boundary is moved laterally until an approximate match is found at a distance of 1,000 m. Figure S12 shows that the simulated pressure response at 173 m bgs is quite similar to the measured pressure data. This step also confirms that our derived permeability estimates are reasonable with respect to allowing long-distance pressure transmission through the fractured basalt. Higher mesh resolution and tighter tolerances will likely allow us to reduce numerical gas pressure dispersion and move the atmospheric boundary farther from the 173-m port in borehole 54-24399, closer to known outcrops in White Rock

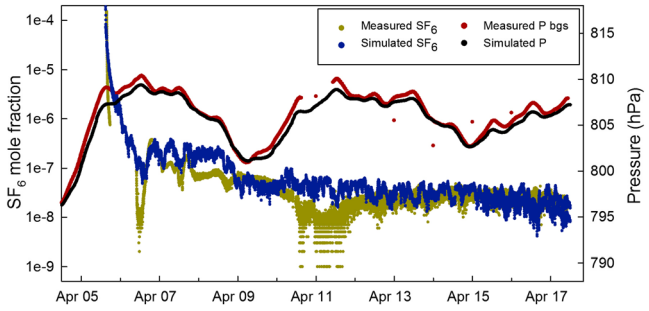

Figure 3. Data versus simulation results at 173 m bgs for SF_6 concentration and pressure. Dark teal is measured borehole concentration. Light teal is simulated concentration. Also shown are measured pressure (red) and simulated pressure (gold).

canyon to the east. However, locating the outcrop responsible for the measured pressure response is beyond the scope of our current analysis. Regardless of the exact outcrop location, the creation of a numerical representation of the correct pressure response driven at a large distance allows us to simulate gas transport behavior associated with the tracer test.

4.5. Simulated Gas Tracer Response

Next, we simulate the tracer test by injecting SF_6 into the 173-m port, following the timeline of the experiment, including chasing the injection with 20 L of surface air and pulling samples at a constant 1 L/min. Parameters that were varied include the longitudinal and transverse dispersivity, the gas diffusion coefficient, and the initial amount of tracer remaining within the simulation domain. The best fit tracer response is shown in Figure 3, where concentration is expressed in parts per part, such that 1e − 6 is 1 μmol/mol. The simulation results are not expected to exactly capture the measured response due to the reduced complexity in the simulated domain compared to the physical system. There are many heterogeneities in the subsurface at this site that contribute to uncertainty and nonideal fit of the tracer solution, such as caves/holes, areas with no/very little overlying tuff layer, or unmapped high-porosity scoria cones—as such, the basalt could in fact be venting to the atmosphere at a number of locations. Three-dimensional heterogeneities such as these cannot be accounted for in our transport model. Thus, the trend of the simulation supports the conceptual model and should lead to the development of more constrained experiments in the future.

For the best fit simulation, longitudinal and transverse dispersivity are found to be 1 and 0.1 m, respectively, near the limit of 0.5 m of estimated numerical dispersion (1/2 the mesh spacing of 1.0 m). Dispersivity of greater than 2 m led to much faster spreading than seen in the data. The simulated porous media gas diffusion coefficient, 3×10^{-6} m^2/s, is based on previous work at this site, and the transport results were not sensitive to this parameter. One major difference between the field data and the simulation is that the simulation requires 90% of the injected mass to be removed from the measurement interval to achieve the fit between simulation and data. We hypothesize that mass was lost down the 27+-m open borehole below the injection port during the injection phase, leaving only a fraction of the injected SF_6 available for transport laterally through barometric pumping. SF_6 has a density that is 5 times higher than air, and would gravitationally separate until its concentration is dilute, approximately 0.1% by mass, or 200 μmol/mol. This hypothesis is supported by the fact that the highest measured concentration immediately after injection of 2 L/min for 10 min (tracer chaser) was 150 μmol/mol at 3:30 pm on 5 April 2017.

4.6. Estimating In Situ Dispersivity

One goal of the simulations is to estimate an effective diffusivity for the basalt based on mechanical spreading induced during barometric pressure changes. In the absence of a velocity field, spreading is caused by simple molecular diffusion. Addition of a velocity field results in hydrodynamic dispersion. As gas velocity increases, dispersion increases through the following relationship relating the average linear velocity (v) to the dispersion coefficient (D) through the dispersivity (α).

$$D = \alpha v + D_{\mathrm{mp}} \tag{1}$$

where D_{mp} is the coefficient of molecular diffusion within the porous medium, and the average linear velocity, v, sometimes termed "pore velocity" or "true velocity," is defined as the volumetric flux divided by porosity (Fetter, 1999; Stauffer, 2006) . An approach to calculate porous media diffusion coefficients is to use the Millington and Quirk (1961) formulation where D_{mp} is a function of porosity (φ) and air content (θ) as

$$D_{\mathrm{mp}} = \frac{D_{\mathrm{free}}\theta^{10/3}}{\phi^2} \tag{2}$$

With a free air diffusion coefficient of SF_6 on the order of 1×10^{-5} m^2/s, and assuming air-filled porosity in the rubblized basalt to be 35%, this function yields a value of 2.5×10^{-6} m^2/s for the molecular diffusion

coefficient in the rubblized basalt. From equation (1), the dispersion coefficient can easily increase above pure molecular diffusion as average linear velocity increases.

Dispersivity in the direction of flow (longitudinal) follows a very approximate 1/10 flow length relationship, while dispersivity in the direction perpendicular to flow (transverse) is often taken to be 1/100 the flow length. These ratios of 1/10 and 1/100 are based on field-scale contaminant plume data that reveal increased spreading with longer-distance transport (Fetter, 1999); however, they serve as guidelines rather than a strict relationship.

To calculate possible increased mass transport from dispersion, one needs both an estimate of the velocity of the gas and the dispersivity (Auer et al., 1996). Through simulation, we determined that a longitudinal dispersivity of 1 m led to spreading that could match observations. Further, using permeability and porosity that fit the pressure response, average linear velocity of the gas near the injection/sampling port can be determined. The dispersion coefficient is calculated using simulated volumetric flux and assigned porosity (Figure S13). Although the massive basalt appears to have a very large impact on spreading, the total mass flowing in these layers is limited by the very low assigned porosity of 0.4%. In the rubblized basalt, the much higher porosity (35%) dominates mass transfer. However, even in the high-porosity basalt, the dispersion coefficient ranges well above pure diffusive transport ($<2.5e-6$ m^2/s). Thus, barometrically pumped gases in the Cerros del Rio basalt are likely seeing 10 to 100 times more mixing than standard diffusive theory would predict in the absence of barometric pumping. With a longitudinal dispersivity of 1 m, the dispersion coefficient (Figure S13) is also the absolute value of the magnitude of the average linear velocity (v). Figure S13 also converts the average linear velocity into more intuitive units of meters per day, showing that gas molecules may be traveling laterally in the rubblized basalt at speeds greater than 10 m/day, with peak velocities reaching above 20 m/day. Within the massive basalt fractures, estimates of average linear velocity are dramatically higher, with short-duration peak values reaching nearly 1,000 m/day.

5. Discussion

5.1. Conceptual Model

In our conceptual model, barometric low pressure pulls a packet of VOCs downward from the Bandelier tuff into the Cerros del Rio basalts. The downward pressure gradient from the Bandelier tuff into the basalts develops because the lower permeability in the Bandelier Tuff phase-shifts the pressure low to a later time and a lower amplitude (Figure S15). As the organic vapor moves vertically downward from the tuff to the basalt, the pressure gradient within the basalt acts to pull the vapors toward the atmospheric connection. Although the figure shows horizontal flow vectors within the basalt, there likely are vertical components to these flow paths caused by the heterogeneity in the layers of rubblized and massive basalt and effects related to the three-dimensional atmospheric boundary. As atmospheric pressure rises, flow paths reverse and air flows back into the basalt. The packet of higher concentration that was pulled into the basalt during the atmospheric low now is transported laterally, with some possible vertical component. Transport leads to spreading and dispersion of the packet. Longer, deeper lows in barometric pressure should push larger packets of VOC mass into the basalt and, subsequently, be pulled out toward the atmospheric boundary.

5.2. Conclusion

Fluctuating SF_6 concentrations observed during tracer testing in a deep fractured basalt demonstrate a strong connection between atmospheric pressure and deep subsurface pressure at the site. These data suggest that the site is impacted by barometric pumping, a phenomenon in which gases may be pulled and spread through the subsurface by barometric pressure fluctuations. Barometric pumping has major implications here and at other sites in fractured media where pressure fluctuations induce rapid gas migration through the subsurface. Our results have implications for the migration of gases linked to a range of scientific problems, including stable isotope analysis (Kwicklis et al., 2006), subsurface nuclear detonation gas migration (Jordan et al., 2015), and contaminated site remediation (Neeper & Stauffer, 2012a, 2012b; You et al., 2011). At contaminated sites, increased gas dispersion may accelerate site remediation in certain cases, but could be problematic in scenarios in which gases are spread toward the water table. The qualitative and quantitative models described in this paper provide a framework for future work exploring gas

migration scenarios under fluctuating pressure conditions, and demonstrate that barometric impacts on gas transport may be important at distances greater than 1 km from atmospheric boundaries.

Acknowledgments
The initial tracer test and analysis was funded through LANL's Environmental Management project. Refinement of the analysis was supported by National Nuclear Security Administration Office of Defense Nuclear Nonproliferation Research and Development and the Defense Threat Reduction Agency. Los Alamos National Laboratory completed this work under the auspices of the U.S. Department of Energy under contract DE-AC52-06NA24596. Data needed to recreate these results are included in Data S1–S5 in the supporting information.

References

Auer, L. H., Rosenberg, N. D., Birdsell, K. H., & Whitney, E. M. (1996). The effects of barometric pumping on contaminant transport. *Journal of Contaminant Hydrology*, *24*(2), 145–166. https://doi.org/10.1016/S0169-7722(96)00010-1

Behar, H. R., Snyder, E. E., Marczak, S., Salazar, L. J., Fordham, G. F., Chu, S. P., et al. (2018). An investigation of plume response to soil vapor extraction and hypothetical drum. *Vadose Zone Journal*. https://doi.org/10.2136/vzj2018.04.0080

Bourret, S. M., Kwicklis, E. M., Miller, T. A., & Stauffer, P. H. (2018). Evaluating the importance of barometric pumping for subsurface gas transport near an underground nuclear test site. *Vadose Zone Journal*, *18*(1). https://doi.org/10.2136/vzj2018.07.0134

Broxton, D. E., & Vaniman, D. T. (2005). Geologic framework of a groundwater system on the margin of a rift basin, Pajarito Plateau, north-central New Mexico. *Vadose Zone Journal*, *4*(3), 522–550. https://doi.org/10.2136/vzj2004.0073

Carrigan, C. R., Heinle, R. A., Hudson, G. B., Nitao, J. J., & Zucca, J. J. (1996). Trace gas emissions on geological faults as indicators of underground nuclear testing. *Nature*, *382*, 528–531. https://doi.org/10.1038/382528a0

FEHM (2019). Accessed on March 6, 2019. https://fehm.lanl.gov/

Fetter, C. W. (1999). *Contaminant Hydrogeology* (2nd ed.). Upper Saddle River, NJ: Prentice Hall.

Harp, D. R., Ortiz, J. P., Pandey, S., Karra, S., Anderson, D., Bradley, C. R., & Stauffer, P. H. (2018). Pore-water storage enhancements and retardation of gas transport in fractured rock. *Transport in Porous Media*, *124*(2).

Johnson, P. J., Otto, S., Weaver, D. J., Dozier, B., Miller, T. A., Jordan, A. B., et al. (2019). Heat-generating nuclear waste in salt: Field testing and simulation. *Vadose Zone Journal*, *18*(1). https://doi.org/10.2136/vzj2018.08.0160

Johnson, P. J., Zyvoloski, G. A., & Stauffer, P. H. (2019). Impact of a porosity-dependent retention function on simulations of porous flow. *Transport in Porous Media*, *127*(1), 211–232. https://doi.org/10.1007/s11242-018-1188-x

Jordan, A. B., Stauffer, P. H., Knight, E. E., Rougier, E., & Anderson, D. N. (2015). Radionuclide gas transport through nuclear explosion-generated fracture networks. *Scientific Reports*, *5*(1), 18383. https://doi.org/10.1038/srep18383, https://www.nature.com/articles/srep18383

Jordan, A. B., Stauffer, P. H., Zyvoloski, G. A., Person, M. A., MacCarthy, J. K., & Anderson, D. N. (2014). Uncertainty in prediction of radionuclide gas migration from underground nuclear explosions. *Vadose Zone Journal*, *13*(10). https://doi.org/10.2136/vzj2014.06.0070

Kuang, X., Jiao, J. J., & Li, H. (2013). Review on airflow in unsaturated zones induced by natural forcings. *Water Resources Research*, *49*, 6137–6165. https://doi.org/10.1002/wrcr.20416

Kwicklis, E. M., Wolfsberg, A. V., Stauffer, P. H., Walvroord, M. A., & Sully, M. J. (2006). Multiphase Multicomponent Parameter Estimation for Liquid and Vapor Fluxes in Deep Arid Systems Using Hydrologic Data and Natural Environmental Traces. *Vadose Zone Journal*, *5*, 934–950.

Martinez, M. J., & Nilson, R. H. (1999). Estimates of barometric pumping of moisture through unsaturated fractured rock. *Transport in Porous Media*, *36*(1), 85–119. https://doi.org/10.1023/A:1006593628835

Millington, R., & Quirk, J. (1961). Permeability of porous solids. *Transactions of the Faraday Society*, *57*, 1200–1207. https://doi.org/10.1039/tf9615701200

Mourzenko, V. V., Varloteaux, C., Guillon, S., Thovert, J.-F., Pili, E., & Adler, P. M. (2014). Barometric pumping of a fractured porous medium. *Geophysical Research Letters*, *41*, 6698–6704. https://doi.org/10.1002/2014GL060865

Neeper, D. A. (2002). Investigation of the vadose zone using barometric pressure cycles. *Journal of Contaminant Hydrology*, *54*(1-2), 59–80. https://doi.org/10.1016/S0169-7722(01)00146-2

Neeper, D. A., & Stauffer, P. H. (2012a). Transport by oscillatory flow in soils with rate-limited mass transfer: 1. Theory. *Vadose Zone Journal*, *11*(2). https://doi.org/10.2136/vzj2011.0093

Neeper, D. A., & Stauffer, P. H. (2012b). Transport by oscillatory flow in soils with rate-limited mass transfer: 2. Field experiment. *Vadose Zone Journal*, *11*(2). https://doi.org/10.2136/vzj2011.0094

Nilson, R. H., Peterson, E. W., Lie, K. H., Burkhard, N. R., & Hearst, J. R. (1991). Atmospheric pumping: A Mechanism causing vertical transport of contaminated gases through fractured permeable media. *Journal of Geophysical Research*, *96*(B13), 21,933–21,948.

Rossabi, J. (2006). Analyzing barometric pumping to characterize subsurface permeability. In C. K. Ho & S. W. Webb (Eds.), *Gas Transport in Porous Media* (pp. 279–290). Springer.

Scotter, D. R., & Raats, P. A. C. (1968). Dispersion in porous mediums due to oscillating flow. *Water Resources Research*, *4*(6), 1201–1206. https://doi.org/10.1029/WR004i006p01201

Scotter, D. R., Thurtell, G. W., & Raats, P. A. C. (1967). Dispersion resulting from sinusoidal gas flow in porous materials. *Soil Science*, *104*(4), 306–308. https://doi.org/10.1097/00010694-196710000-00012

Stauffer, P. H. (2006). Flux flummoxed: A proposal for consistent usage. *Groundwater*, *44*(2), 125–128. https://doi.org/10.1111/j.1745-6584.2006.00197.x

Stauffer, P. H., Birdsell, K. H., Witkowski, M. S., & Hopkins, J. K. (2005). Vadose zone transport of 1,1,1-trichloroethane: Conceptual model validation through numerical simulation. *Vadose Zone Journal*, *4*(3), 760–773. https://doi.org/10.2136/vzj2004.0120

Vesselinov, V. V., Keating, E. H., & Zyvoloski, G. A. (2002). Analysis of model sensitivity and predictive uncertainty of capture zones in the Espanola Basin regional aquifer, Northern New Mexico, Los Alamos National Laboratory; LA-UR-02, Los Alamos, NM.

Weeks, E. P. (2001). *Effect of Topography on Gas Flow in Unsaturated Fractured Rock: Concepts and Observations*, *Geophysical Monograph Series* (Vol. 42, pp. 53–59). Washington, DC: American Geophysical Union. https://doi.org/10.1029/GM042p0053

Witherspoon, P. A., Wang, J. S. Y., Iwai, K., & Gale, J. E. (1980). Validity of cubic law for fluid-flow in a deformable rock fracture. *Water Resources Research*, *16*(6), 1016–1024. https://doi.org/10.1029/WR016i006p01016

You, K., & Zhan, H. (2013). Comparisons of diffusive and advective fluxes of gas phase volatile organic compounds (VOCs) in unsaturated zones under natural conditions. *Advances in Water Resources*, *52*, 221–231. https://doi.org/10.1016/j.advwatres.2012.11.021

You, K., Zhan, H., & Li, J. (2011). Gas flow to a barometric pumping well in a multilayer unsaturated zone. *Water Resources Research*, *47*, W05522. https://doi.org/10.1029/2010WR009411